ORGANOMETALLICS

Article

pubs.acs.org/Organometallics

Efficient Hydrosilylation of Acetophenone with a New Anthraquinonic Amide-Based Iron Precatalyst

Álvaro Raya-Barón,[†] Manuel A. Ortuño,[‡] Pascual Oña-Burgos,[†] Antonio Rodríguez-Diéguez,[§] Robert Langer,[∥] Christopher J. Cramer,*[,‡] Istemi Kuzu,*[,∥] and Ignacio Fernández*[,†,⊥]

[†]Department of Chemistry and Physics, ceiA3, Universidad de Almería, Ctra. Sacramento, s/n, E-04120 Almería, Spain

[‡]Department of Chemistry, Chemical Theory Center, and Supercomputing Institute, University of Minnesota, Minneapolis, Minnesota 55455-0431, United States

[§]Department of Inorganic Chemistry, Faculty of Science, University of Granada, 18070 Granada, Spain

[∥]Fachbereich Chemie, Philipps-Universität Marburg, Hans-Meerwein-Straße 4, 35032 Marburg, Germany

[⊥]BITAL, Research Centre for Agricultural and Food Biotechnology, Ctra. Sacramento, s/n, E-04120 Almería, Spain

Supporting Information

ABSTRACT: A new iron complex based on a noninnocent anthraquinonic ligand has been synthesized and fully characterized through multiple techniques, including NMR, X-ray crystallography, mass spectrometry, and cyclic voltammetry. Exposure of ketone to that complex in the presence of $(EtO)_2MeSiH$ affords the corresponding silylated alcohol. Loadings as low as 0.25 mol % afford excellent yields at room temperature. Quantum−chemical analysis of the catalytic mechanism supports activation of the precatalyst to form a Fe−hydride intermediate, followed by ketone reduction and σ-bond metathesis.

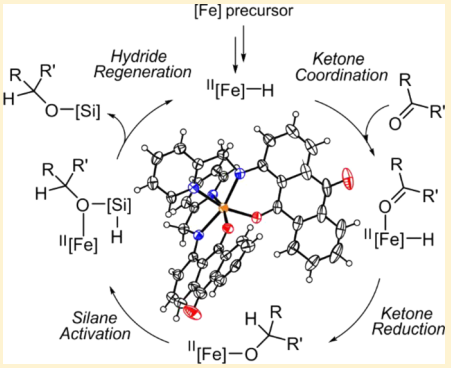

The hydrosilylation of carbonyl groups is an important synthetic transformation and one that is often used to evaluate specific catalysts for potential further utility if engineered to accomplish CO_2 reduction.[1] Hydrosilylation combines reduction of the carbonyl functionality with alcohol protection in a single step, where the most common and active catalysts are based on precious metals.[2] In the past decade, much effort has been dedicated to the development of catalysts based on earth-abundant metals, which has opened unprecedented routes for molecular functionalization.[3] Iron, in particular, has been exploited because of its benign environmental impact, high abundancy in nature, and low price, and has emerged as one of the most noteworthy substitutes in the catalyzed hydrosilylation.[4−6] From a mechanistic perspective, there are few contributions dealing with this transformation, mostly on low-spin iron(II) hydride catalysts.[3d,4a,e,f,i,5−8] Very recently, Gade and co-workers have given insights in the mechanism of chiral iron carboxylate precatalysts,[5,9] identifying a rate-determining σ-bond metathesis step of the complex with the silane, subsequent coordination of a ketone to the iron hydride complex, and finally an insertion of the ketone into the Fe−hydride bond to regenerate the active species.

Herein, we report the synthesis and characterization of a new anthraquinonic amide-base complex that includes two nitrogen atoms in the tridentate ligand. Preliminary results and computational mechanistic studies on the hydrosilylation of acetophenone catalyzed by the new complex are also presented.

The ligand containing an N-heterocyclic chelating element has been synthesized from common, inexpensive starting materials in high yields, from the reaction of chloroanthraquinone with 2-picolylamine at 150 °C over short reaction times. The isolated yield is 40% (see Supporting Information for NMR, mass spectrometry, IR, and X-ray crystallographic data). A key identifying feature in the ^1H NMR spectra of the ligand is the presence of a broad triplet NH resonance at δ_H 10.50 ppm, due to hydrogen-bonding with the C═O moiety, together with the doublet associated with the methylene bridge (δ_H 4.84 ppm). $^1H,^{15}N$ HMQC experiments optimized for $1/2J_{NH}$ of 83.3 ms (Figure S15) permitted the assignment of two nitrogens at δ_N 77.9 (NH) and 307.0 ppm for the picolyl and pyridine units, respectively. The former interacts exclusively with the NH proton, while the latter shows cross peaks with its vicinal proton and the methylenic moiety. The X-ray crystal structure of **1** (Figure 1), grown by hexane diffusion in a dicloromethane solution, confirms the chelating potential of the ligand given the intramolecular hydrogen bond between NH and C═O (quinone) of 2.629 Å (Figures 1 and S26). This

Received: October 1, 2016

DOI: 10.1021/acs.organomet.6b00765
Organometallics XXXX, XXX, XXX−XXX

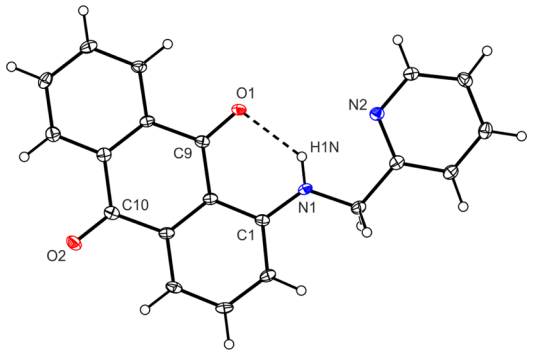

Figure 1. Molecular structure of ligand **1** determined from single-crystal X-ray diffraction. Thermal ellipsoids are shown at the 30% probability level.

interaction produces a slightly longer carbonyl bond (C9−O1, 1.238(2) Å) than that found for the non-hydrogen-bonded case (C10−O2 1.227(2) Å). In the crystal network, anthraquinone moieties of **1** are oriented in a face-to-face manner with an interplanar distance of ca. 3.4 Å, establishing π-stacking arrangements (Figures S27−28). This interaction induces architecturally controlled self-assembly, leading to molecular aggregates in the solid state, as has been described previously.[10]

The reaction of **1** with 0.5 equiv of $Fe(HMDS)_2$ in THF led to quantitative formation of complex **2** (Scheme 1).

Scheme 1. Synthesis of Anthraquinonic Iron Complexes 2 and 3[a]

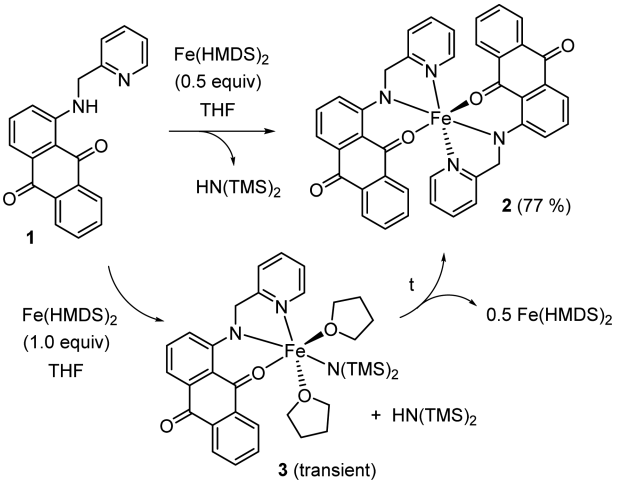

[a]See the Supporting Information for more details. We tentatively assume that two THF molecules complete the coordination sphere of iron in complex **3**.

Interestingly, when the reaction between ligand **1** and $Fe(HMDS)_2$ is performed using a 1:1 molar ratio (ligand:Fe precursor), complex **3** is initially obtained (Scheme 1), which progressively disappears forming again complex **2**. NMR monitoring of the 1:1 stoichiometry reaction (Figure S18) indicated that after 12 h under these conditions quantitative conversion to complex **2** is achieved.

Thus, there is a thermodynamic equilibrium between complexes **2** and **3**, with the former being the thermodynamically more stable species. For ligand/iron stoichiometries greater than 2:1, e.g., 3:1 or 4:1, the ^{1}H NMR spectra showed the coexistence of complex **2** and free ligand in agreement with a stable complex not prone to dissociation and/or aggregation on the NMR time scale. Despite their paramagnetism, the ^{1}H NMR spectra of complexes **2** and **3** reported in this work are informative and have been partially assigned.

Complex **2** proved to be stable in THF solution over several weeks without any sign of decomposition. The THF-d_8 ^{1}H NMR spectrum of **2** at 23 °C exhibits a number of resonances consistent with a paramagnetic C_{2v}-symmetric iron complex having resonances shifted over a 200 ppm range.[11] Variable temperature ^{1}H NMR spectra and a list of diagnostic signals are provided in the Supporting Information. In general, the in-plane hydrogens on the chelate exhibit relatively large deviations from their diamagnetic reference values. In THF-d_8, the pyridine protons are observed as rather broad downfield peaks at δ_H 154.4 ($W_{1/2}$ = 3019 Hz) and 136.8 ppm ($W_{1/2}$ = 2375 Hz). The three closer to the iron anthraquinone protons resonate at δ_H 85.4, 57.4, and 35.9 ppm, while the most remote appeared as sharper singlets located at δ_H 37.7 ($W_{1/2}$ = 43 Hz), 27.1 ($W_{1/2}$ = 84 Hz), and −28.2 ppm ($W_{1/2}$ = 98 Hz). Transient complex **3** shows a number of resonances consistent with a C_s paramagnetic complex with higher and lower frequency signals located at δ_H 189.2 and −34.1 ppm, respectively. Accordingly, the ^{1}H NMR spectrum in THF-d_8 at 23 °C exhibits diagnostic resonances with large isotropic shifts for the in-plane hydrogens (Figure S17). The Evans method was used to calculate the solution magnetic susceptibility values, χ_M, for complex **2**, giving rise to a number of unpaired electrons (n = 4) consistent with a high-spin Fe(II) electronic configuration (see Supporting Information and Figure S25). The FT-IR spectra (Figure S21) showed two C═O stretching bands at 1641 and 1580 cm^{-1}, indicating the unsymmetrical coordination of the two quinone oxygens. As far as we are aware, this is the first example of an anthraquinonic amide-based iron complex described to date.

Purple single crystals were obtained from layering with *n*-pentane a THF solution of complex **2** at room temperature. The same compound was obtained when using dichloromethane instead of THF. The two crystallized compounds (**2** in THF, and **2b** in dicloromethane) are essentially the same but with different crystallization solvents included in the lattice (see Supporting Information). The geometry about Fe can best be described as a distorted octahedron with two tridentate ligands bound to the metal with four nitrogens (two pyridinic and two amidic) and two weakly interacting carbonyl oxygens (Figure 2). Bond angles of 170.50(6), 78.70(5), and 94.58(5)°, are observed for N(1)−Fe(1)−N(3), N(1)−Fe(1)−N(2), and O(1)−Fe(1)−O(3) respectively (Figure 2).

Inspection of the anthraquinone chelate carbonyl C═O distances reveals considerable elongation [1.268(2) and 1.2646(19) Å] relative to that of the uncomplexed carbonyls [1.232(2) and 1.228(2) Å], consistent with NMR and IR data. Corresponding bond distances and angles are given in Tables S2 and S3. The positive ion mode ESI mass spectrum reveals a parent ion corresponding to $[\mathbf{2}]^+$ m/z 682.1296 (Figure S23), confirming its full integrity in the gas phase. The observed isotope pattern matches well with that calculated for the exact mass of $[C_{40}H_{26}FeN_4O_4]$ (Figures S23 and 24).

The redox properties of complex **2** were investigated by cyclic voltammetry in dichloromethane. The redox potentials are given versus the standard Fc/Fc^+ couple. The first reversible one-electron reduction of the anthraquinone moiety in complex **2** to the corresponding radical anion was observed at ca. −0.85 V vs Fc/Fc^+ couple. The irreversible reduction wave at −1.37 V

DOI: 10.1021/acs.organomet.6b00765
Organometallics XXXX, XXX, XXX−XXX

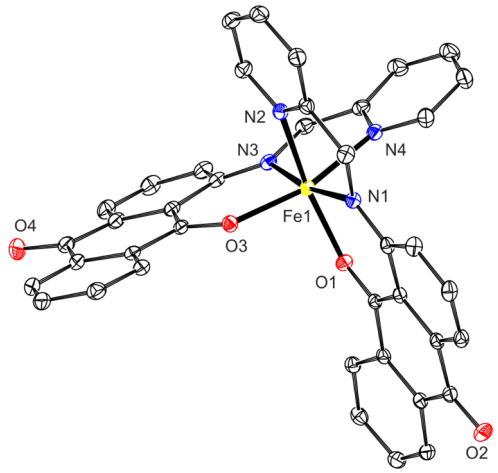

Figure 2. Molecular structure of complex **2** determined from single-crystal X-ray diffraction. Thermal ellipsoids are shown at the 30% probability level. Hydrogen atoms are omitted for clarity.

in the cyclic voltammogram of **2** is assignable to a second reduction of the anthraquinone-based ligand in **2**. In comparison to those of the uncoordinated ligand (**1**) the observed redox couples of the anthraquinone moiety in **2** are shifted by +0.58 and +0.65 V upon coordination to iron(II) (Figure 3). While the voltammogram of **1** exhibits distinct

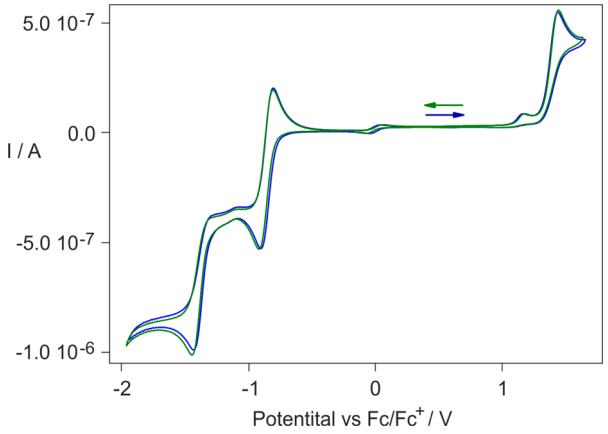

Figure 3. Cyclic voltammogram of complex **2** in CH_2Cl_2 with different scan directions (1 mM, scan rate 100 mV/s, Pt//0.1 M nBu$_4$NPF$_6$// Pt).

redox couples at 0.80 and 1.10 V, which are in line with amine- and pyridine-oxidation, respectively, complex **2** shows an irreversible oxidation process at 1.38 V that we assign to Fe^{II}/Fe^{III}-couple.

We were glad to find that complex **2** could be prepared in THF from the reaction of $Fe(OAc)_2$ (or alternatively $FeCl_2$), ligand **1**, and LiHMDS in a ratio 1:2.2:2, respectively (see Supporting Information). These routes were important in order to use a much more convenient iron source in catalysis. With the new iron complex fully characterized in solution and the solid state, we tested its efficiency for the hydrosilylation of acetophenone (Table 1). Stirring the reaction mixture at room temperature for 1 h followed by workup afforded the corresponding alcohol in 52 and 3% yields, when using silanes EtO_2MeSiH or Ph_2SiH_2, respectively (entries 1 and 3). Interestingly, at longer reaction times (entries 2, 4, and 5)

Table 1. Hydrosilylation of Acetophenone Catalyzed by 2[a]

entry	Fe prec.	**1** (equiv)	silane	t (h)	conv. (%)
1[b]	**2**		$(EtO)_2MeSiH$	1	52
2	**2**		$(EtO)_2MeSiH$	24	80 (90)[e]
3	**2**		Ph_2SiH_2	1	3
4	**2**		Ph_2SiH_2	24	45
5	**2**		Ph_2SiH_2	62	96
6[c]	$Fe(OAc)_2$	2.2	$(EtO)_2MeSiH$	1	77
7[c]	$FeCl_2$	2.2	$(EtO)_2MeSiH$	1	50
8	$Fe(OAc)_2$		$(EtO)_2MeSiH$	24	0
9	$FeCl_2$		$(EtO)_2MeSiH$	24	0
10[d]	**2**		$(EtO)_2MeSiH$	1	50
11[d]	**2**		$(EtO)_2MeSiH$	24	85
12[d]	**2**		Ph_2SiH_2	24	72
13[d]	**2**		Ph_2SiH_2	62	96
14	**2**		Et_3SiH	24	0
15[c]	$Fe(OAc)_2$	2.2	Et_3SiH	24	0
16	**2**		Ph_3SiH	24	0
17[c]	$Fe(OAc)_2$	2.2	Ph_3SiH	24	0

[a]Reaction conditions unless stated otherwise: acetophenone (2 mmol), hydrosilane (2.5 mmol), Fe precursor (0.25 mol %), LiHMDS (base), THF (6 mL), room temperature. Quenched with 1 M HCl (aqueous). Conversions determined by crude ^{1}H NMR. See Supporting Information. [b]When the reaction is performed in absence of THF, the same conversion is obtained. [c]Two equivalents of LiHMDS were employed. [d]Addition of LiOAc (2 equiv). [e]In parentheses are shown the conversions when using 0.5 mol % of catalyst.

the catalytic reactions proceed quantitatively, although the use of Ph_2SiH_2 requires about three times longer to proceed with excellent yields. When complex **2** is prepared *in situ* from $Fe(OAc)_2$ in the reaction vessel (entry 6), the conversion is notably higher than when using **2** in isolated form. Under these conditions, the presence of the amide ligand is required in order to observe catalysis (entries 8 and 9). The hydrosilylation of ketones catalyzed by a combination of $Fe(OAc)_2$ with various N-coordinating ligands has been reported previously by Nishiyama and Furuta[6] but with reaction temperatures of 65 °C and loadings of catalysts above 5%. The substitution of the acetate precursor by $FeCl_2$ (entry 7) produced the same catalytic outcome as when using complex **2** in isolated form. The higher yields from *in situ* generated catalyst (entry 1 vs entry 6) encouraged us to employ complex **2** in the presence of LiOAc as an initiator. The yields are shown in entries 10−13 and showed no significant improvement for either EtO_2MeSiH or Ph_2SiH_2. Neither triethylsilane nor triphenylsilane displayed any reactivity under isolated or *in situ*-generated catalytic conditions (entries 14−17). We attribute this to the lesser hydridic characters for these less Si−H polarized reagents.[12]

The estimated TOF values for complex **2** were 3.5 min^{-1} (entry 1, Table 1) and 5.1 min^{-1} (entry 6, Table 1). To place these activities in context, it is fair to evoke the calculated TOF values for some of the most active iron complexes in the same transformation. In this sense, special mention is given to that reported by Ruddy et al. (393 min^{-1})[4g] or that described by Yang and Tilley (~10 min^{-1}).[4d] A comparison of prominent first-row metal catalysts has been provided by Trovitch and co-workers.[13] Importantly, in our case no special neutral donor ligand or activator is required. It is noteworthy that all reactions were conducted at room temperature, illustrating the useful activity of the catalysts described herein.

DOI: 10.1021/acs.organomet.6b00765
Organometallics XXXX, XXX, XXX−XXX

We now turn to electronic structure calculations to investigate the reaction mechanism. The hydrosilylation of acetophenone described in entry 6 of Table 1 has been modeled at the density functional theory (DFT) level (see Computational Details). Starting from the precatalyst **2**, we have removed one anthraquinonic ligand to create available coordination sites to catalyze reactivity (Figure 4a). We have

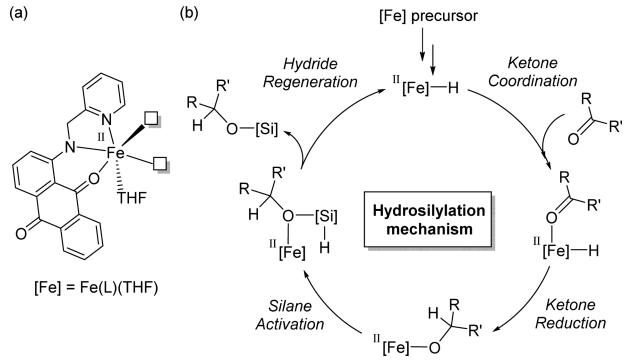

Figure 4. (a) Active species and (b) general reaction mechanism for Fe(II)-catalyzed hydrosilylation of ketones.

also considered one additional explicit THF molecule solely to complete the coordination sphere, since no major role is expected (Table 1, entry 1, footnote b). For the silane, ethoxy is replaced by methoxy for computational efficiency. All Fe(II) complexes are high-spin (quintet).[14] All energies correspond to 298 K Gibbs free energies in THF solution in kcal mol^{-1}.

In line with previous studies,[4e,i,7,9,12,15] we propose the participation of an Fe(II)−hydride as an active species in the catalytic cycle (Figure 4b), which proceeds as (i) coordination and reduction of the ketone, (ii) silane activation, and (iii) Fe−hydride regeneration and product release (see Lewis acid mechanism in Figure S40).

The computed reaction mechanism is shown in Scheme 2, where separated Fe−hydride **5** and relevant reagents are taken as the zero of free energy. The first step of the reaction entails

Scheme 2. Computed Reaction Mechanisms[a]

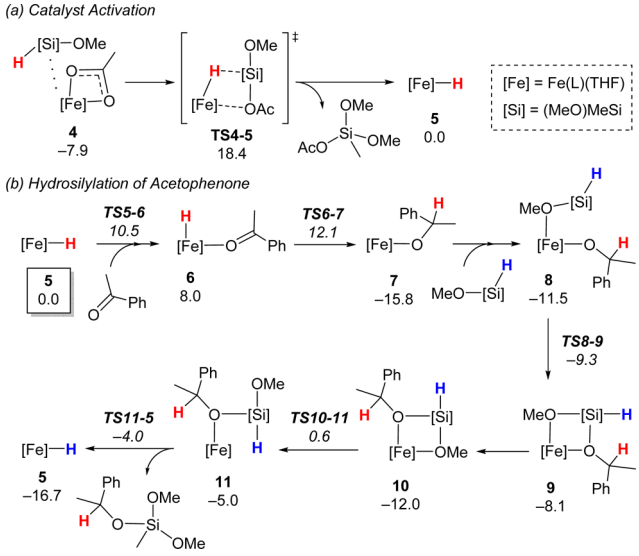

[a](a) Catalyst activation and (b) hydrosilylation of acetophenone. ΔG_{THF} in kcal mol^{-1}.

activation of the catalyst (Scheme 2a). We start from a van der Waals complex of [Fe(κ^2-AcO)] and silane **4** (−7.9 kcal mol^{-1}), which undergoes σ-bond metathesis via **TS4−5** (18.4 kcal mol^{-1}) to generate the hydride **5**.

In the subsequent hydrosilylation catalytic cycle (Scheme 2b), ketone coordination takes place via **TS5−6** (10.5 kcal mol^{-1}), followed by insertion via **TS6−7** (12.1 kcal mol^{-1}) (see isomer in Figure S41a), which reduces the carbonyl group producing alkoxide **7** (−15.8 kcal mol^{-1}). Next, silane coordinates to iron via **TS8−9** (−9.3 kcal mol^{-1}) to form a 5-coordinate silicon atom in **9** (−8.1 kcal mol^{-1}). Further conformational rearrangements exchanging the methoxy and alkoxide positions generates complex **10** that is in equilibrium with a higher energy agostic-like complex **11** via **TS10−11** (0.6 kcal mol^{-1}) (see isomer in Figure S41b). The latter can undergo σ-bond metathesis via **TS11−5** (−4.0 kcal mol^{-1}) to regenerate the hydride **5** and release the protected alcohol.

In the above mechanistic scenario, the anthraquinonic ligand is only a spectator, but we did consider its possible participation in the proposed reaction mechanism. As shown in Scheme 2b, the transition state **TS6−7** features a hydride insertion into the carbonyl of the substrate at 12.1 kcal mol^{-1}. In this line, the anthraquinonic ligand also contains a carbonyl group that might be reduced. Computed transition state **TS6−L** that describes the hydride insertion into the anthraquinonic carbonyl is found at 27.7 kcal mol^{-1} above **5**, i.e., this step requires 15.6 kcal mol^{-1} more than the hydride insertion into the substrate via **TS6−7**. Although the process cannot be completely ruled out, it is unfavorable and nonproductive toward catalysis.

The overall Gibbs free energy profile is shown in Figure 5. Silane activation and Fe−hydride regeneration taken in

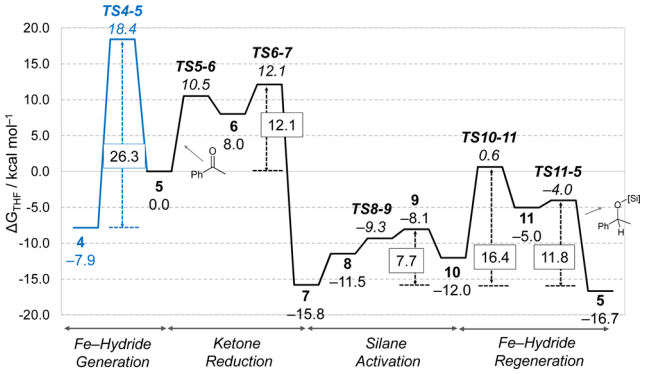

Figure 5. Gibbs energies along reaction coordinate for Fe-catalyzed hydrosilylation of acetophenone.

sequence comprise σ-bond metathesis. The associated free energy of activation for this process ($\Delta G^{\ddagger}$ = 16.4 kcal mol^{-1} relative to **7**) is higher than that of ketone reduction ($\Delta G^{\ddagger}$ = 12.1 kcal mol^{-1} relative to **5**). In the analogous process reported by Bleith and Gade[9] for a different iron-based catalyst reacting with acetophenone and $(MeO)_2MeSiH$, the computed free energy of activation for σ-bond metathesis is similar ($\Delta G^{\ddagger}$ = 12.0 kcal mol^{-1} compared to $\Delta G^{\ddagger}$ = 11.8 kcal mol^{-1} (**TS11−5** relative to **7**)), but the free energy of activation computed for ketone reduction was considerably lower ($\Delta G^{\ddagger}$ = 6.9 kcal mol^{-1} compared to $\Delta G^{\ddagger}$ = 12.1 kcal mol^{-1} (**TS6−7** relative to **5**)), presumably owing to the greater Lewis acidity of their iron complex facilitating the first step. This suggests that next-generation design within the context of our own ligand system might be to substitute the pyridyl ring with electron-

DOI: 10.1021/acs.organomet.6b00765
Organometallics XXXX, XXX, XXX−XXX

withdrawing functionality to similarly accelerate ketone reduction.

The relatively small computed free energy of activation for the catalytic cycle involving **5** is consistent with the observed efficiency and mild conditions for the experimental process. We note that the activation free energy for initial catalyst activation ($\Delta G^{\ddagger}$ = 26.3 kcal mol^{-1} from **4** through **TS4−5**)[16] is actually larger than the turnover-limiting step for catalysis; thus, an induction period prior to catalysis is expected, which has been reported by Bleith and Gade as well.[9] Transition-state theory based on the computed results predicts a TOF of 0.42 min^{-1},[17] which is within an order of magnitude of the experimental estimate of 5.1 min^{-1} (entry 6 Table 1).

We may also use computation to predict the kinetic isotope effect (KIE)[18] for catalyst activation (from **4** through **TS4−5**), ketone reduction (from **5** through **TS6−7**), and σ-bond metathesis (from **7** through **TS11−5**). The computed H/D KIE values are 1.88, 1.04, and 1.51, respectively. Whereas the H/D KIE for the catalyst activation step is similar to previous experiments using carboxylate precatalysts,[9] the values for ketone reduction and σ-bond metathesis are somewhat smaller.[19]

In summary, readily accessed, well-defined anthraquinone amide-based iron complexes can be isolated (or prepared *in situ*) as efficient catalysts for the hydrosilylation of carbonyls. The method is usable under very mild conditions and using loadings of catalyst as low as 0.25 mol % with no need for special neutral donors or activators. Calculations suggest a large activation free energy for the catalyst preactivation step to form the initial Fe−hydride, after which ketone reduction and σ-bond metathesis processes occur readily. Further derivatization of the ligand and their use in more challenging catalysis are in progress.

EXPERIMENTAL SECTION

General Information. All experiments were performed under an inert atmosphere of N_2 or argon using standard Schlenk techniques or a glovebox. Deuterated solvents were degassed and dried over activated molecular sieves prior to use. DMSO was dried by distillation from anhydrous CaH_2 and then stored over activated 3 Å molecular sieves. 2-Picolylamine was distilled from KOH under reduced pressure before use. 1-Chloroanthraquinone was purchased from Aldrich and used as received. THF and hexane were dried and degassed in a Solvent Purification System. $Fe(HMDS)_2$ was synthesized by a method previously described in literature.[20] Pentane used for crystallization was dried by distillation from Na/K alloy and stored over 4 Å molecular sieves. LiHMDS, $FeCl_2$, and $Fe(OAc)_2$ were purchased from ABCR and used as received. All hydrosilanes employed in the catalytic runs were purchased from Acros and used without further purification. Acetophenone was distilled from anhydrous $MgSO_4$ under reduced pressure and collected over activated molecular sieves, then degassed. Triethylamine was distilled from CaH_2, degassed, and stored over activated molecular sieves. NMR spectra were measured via Bruker Avance III 300, Bruker Avance III 500, or Bruker Avance III 600 spectrometers. IR spectra were recorded in a FT-IR Bruker Alpha spectrometer. Mass spectra were acquired with a LTQ-FT Ultra mass spectrometer (Thermo Fischer Scientific). Elemental analyses (EA) were performed on a Elementar vario EL cube in the CHN mode.

Synthesis and Analytical Data for Ligand 1. To a solution of 1-chloroanthraquinone (2.4 g, 9.69 mmol) in DMSO (30 mL) in a Schlenk vessel was added 2-picolylamine (2.50 mL, 24.23 mmol), and the mixture was stirred at 150 °C during 20 min. Then, the solution was poured into cold distilled water (400 mL), and the resulting precipitate was filtered out and washed with distilled water. The pure product was obtained as a red powder after purification through silica gel column using ethyl acetate/hexanes (1:1) as eluent. Yield: 1.23 g (40%). Suitable crystals for X-ray diffraction were grown by layering a solution of **1** in dichloromethane with hexane at 5 °C. Elemental analysis calcd (%) for $C_{20}H_{14}N_2O_2$: C, 76.42; H, 4.49; N, 8.91; found: C, 76.44; H, 4.60; N, 8.73. ^{1}H NMR (600.13 MHz, $CDCl_3$, δ, ppm) 10.49 (1H, bs, N*H*), 8.76 (1H, ddd, *J* = 1.2 Hz, 1.8 Hz, 4.8 Hz, H20), 8.38 (1H, dd, *J* = 0.6 Hz, 7.8 Hz, H8), 8.34 (1H, dd, *J* = 0.6 Hz, 7.8 Hz, H5), 7.86 (1H, ddd, *J* = 1.2 Hz, 7.2 Hz, 7.2 Hz, H7), 7.81 (1H, ddd, *J* = 1.2 Hz, 7.2 Hz, 7.2 Hz, H6), 7.78 (1H, ddd, *J* = 1.8 Hz, 7.8 Hz, 7.8 Hz, H18), 7.72 (1H, dd, *J* = 1.2 Hz, 7.2 Hz, H4), 7.59 (1H, dd, *J* = 8.4 Hz, 8.4 Hz, H3), 7.46 (1H, d, *J* = 7.8 Hz, H17), 7.33 (1H, dd, *J* = 5.4 Hz, 7.2 Hz, H19), 7.11 (1H, dd, *J* = 0.6 Hz, 8.4 Hz, H2), 4.84 (2H, d, *J* = 5.4 Hz, H15). ^{13}C NMR (150.92 MHz, $CDCl_3$, δ, ppm) 185.4 (CO, C9), 183.7 (CO, C10), 157.6 (C16), 151.3 (C1), 149.4 (C20), 137.2 (C18), 135.4 (C3), 134.9 (C12), 134.7 (C14), 134.0 (C7), 133.1 (C6), 133.1 (C11), 126.9 (C8), 126.8 (C5), 122.5 (C19), 121.2 (C17), 118.3 (C2), 116.3 (C4), 113.8 (C13), 48.6 (CH_2, C15). ESI-MS calcd (*m*/*z*) for $C_{20}H_{15}N_2O_2^+$: 315.1128; found: 315.1122 [M + H]$^+$. IR (KBr) ν (cm^{-1}) 3269m, 2923m, 2853m, 1668s, 1635s, 1591s, 1505s, 1481s, 1431s, 1409s, 1298s, 1270s, 1230s, 1001m, 707s.

Synthesis and Analytical Data for Complex 2. A solution of $Fe(HMDS)_2$ (56.4 mg, 0.15 mmol) in THF (10 mL) was added to a suspension of **1** (94.2 mg, 0.30 mmol) in THF (10 mL). The resulting solution was stirred at room temperature for 20 min; then, all the volatiles were removed under reduced pressure. The pure product was obtained as dark purple crystals by layering a THF solution with *n*-pentane. Yield: 79 mg (77%). Crystals can be also grown from layering with *n*-pentane a CH_2Cl_2 solution of complex **2** at room temperature. Complex **2** can be also synthesized using $FeCl_2$ as iron(II) precursor. Thus, a solution of LiHMDS (56.4 mg, 0.32 mmol) in THF (5 mL) was added to a solution of **1** (100 mg, 0.32 mmol) in THF (15 mL). The resulting blue solution was poured upon a suspension of $FeCl_2$ (40.5 mg, 0.16 mmol) in THF (5 mL). Then, triethylamine (177 μL, 0.64 mmol) was added and the mixture stirred during 30 min. After removing all the volatiles under vacuum, dichloromethane was added in order to dissolve **2** and remove LiCl by filtration. Pure crystalline product was obtained after layering *n*-pentane upon a dichloromethane solution. Elemental analysis calcd (%) for $C_{40}H_{26}FeN_4O_4$·(THF): C, 70.03; H, 4.54; N, 7.42; found: C, 69.06; H, 4.52 N, 7.69. ^{1}H NMR (300.13 MHz, THF-d_8, δ, ppm) 154.4 (1H, bs), 136.8 (1H, bs), 85.4 (1H, bs), 57.4 (1H, bs), 37.7 (1H, s), 35.9 (1H, bs), 30.1 (1H, bs), 27.1 (1H, s), 7.4 (1H, s), 7.1 (1H, s), −1.6 (1H, s), −28.2 (1H, s), −31.9 (1H, bs). ESI-MS calcd (*m*/*z*) for $C_{40}H_{26}FeN_4O_4^+$: 682.1303; found: 682.1296 [M]$^+$. IR (ATR) ν (cm^{-1}) 3066w, 2954w, 2925w, 2852w, 1641s, 1580s, 1522m, 1474m, 1410s, 1347s, 1304s, 1246s, 1227s, 994s, 704s, 487s.

Observation of Complex 3. A solution of **1** (43.2 mg, 0.137 mmol) in THF (20 mL) was added to a solution of $Fe(HMDS)_2$·THF (61.7 mg, 0.137 mmol) in THF (5 mL). An aliquot of the resulting blue solution was taken and analyzed through NMR. ^{1}H NMR (300.13 MHz, THF-d_8, δ, ppm) 189.2 (1H, bs), 150.3 (1H, bs), 82.8 (1H, s), 60.1 (1H, s), 45.054 (1H, s), 28.0 (1H, s), 18.2 (18H, bs, HMDS), 11.5 (1H, s), 10.2 (1H, bs), 8.951 (1H, s), −2.3 (1H, s), −2.9 (1H, s), −25.8 (1H, bs), −34.1 (1H, s).

General Procedures for the Catalytic Hydrosilylation of Acetophenone. Inside the glovebox, compound **2** (0.25 or 0.5 mol %) was dissolved in THF (6 mL) inside a vial or a Schlenk tube. The corresponding silane (2.5 mmol) was then added to the solution, followed by acetophenone (2 mmol) and the vial or Schlenk tube sealed. The resulting mixture was stirred at room temperature during the times indicated in Table 1 and then the reaction was quenched by adding 1 M HCl (aqueous, 5 mL) while in an ice bath and stirred long enough to ensure the complete hydrolysis of the silylether. The mixture was then taken to ph 7 by adding 5 M NaOH (aqueous) and the organic products extracted with ethyl acetate (3 × 15 mL). The organic layers were dried using anhydrous Na_2SO_4, filtered, and concentrated by rotatory evaporation. As an alternative method, inside the glovebox, ligand **1** (0.55 mol %) and LiHMDS (0.50 mol %) were dissolved together in THF (6 mL) inside a vial, proving the deprotonation of ligand **1** by the formation of a deep blue solution.

DOI: 10.1021/acs.organomet.6b00765
Organometallics XXXX, XXX, XXX−XXX

This solution was then poured inside another vial containing the appropriate iron(II) precursor (0.25 mol %). To the resulting mixture, the corresponding silane (2.5 mmol) was added, followed by acetophenone (2 mmol) and the vial sealed. The rest of the procedure was identical as that described above.

X-ray Structure Determination. Prismatic crystals of compounds **1**, **2**, and **2b** suitable for X-ray experiments were obtained and resin epoxy coated and mounted on Bruker Axs APEX (**1**) and Stoe IPDS 2T (**2** and **2b**) diffractometers, respectively. Instruments were equipped with graphite monochromated Mo Kα radiation (λ = 0.71073 Å), operating at 50 kV and a temperature of 293 K for **1** and 100 K for **2** and **2b**. The cell parameters were determined and refined by least-squares fit of all reflections collected. An empirical absorption correction was applied. The data reduction was performed with the APEX2[21] software and corrected for absorption using SADABS.[22] Crystal structures were solved by direct methods using the SIR97 program[23] and refined by full-matrix least-squares on F^2 including all reflections using anisotropic displacement parameters by means of the WINGX crystallographic package.[24] In all cases, the hydrogen atoms were included with their calculated positions determined by molecular geometry and refined riding on the corresponding bonded atom. Final $R(F)$, $wR(F^2)$, and goodness of fit agreement factors, details on the data collection, and analysis can be found in Table S1. Cambridge Crystallographic Data Centre numbers are 1493111 (**1**), 1507476 (**2**), and 1514974 (**2b**). These data can be obtained free of charge from The Cambridge Crystallographic Data Centre via www.ccdc.cam.ac.uk/data_request/cif.

Cyclic Voltammetry. For the electrochemical measurements, a temperature-controlled microcell HC (RHD Instruments) was used. The measurements were carried out at 25 ± 0.1 °C in a three-electrode configuration with a polycrystalline Pt wires acting as a pseudoreference and working electrode. A Pt crucible acted as a container for the samples and as the counter electrode with [nBu$_4$N][PF$_6$] (0.1M) as electrolyte. The electrochemical cell was connected to a PGSTAT204 potentiostat/galvanostat (Metrohm Autolab). In order to achieve the same conditions for all measurements, the electrodes were freshly polished, carefully rinsed with acetone and CH_2Cl_2, and finally dried in vacuum. For each sample, the pure electrolyte solution was measured as a control experiment. Ferrocene was used as internal standard, and the reported potentials are referenced to the standard potential of $[(\eta^5\text{-}C_5H_5)_2Fe]/[(\eta^5\text{-}C_5H_5)_2Fe]^+$ (Fc/Fc^+). Furthermore, each redox wave was examined separately at different scan rates, showing a linear dependency of the current versus the square root of the scan rate processes under diffusion control. Table S4 summarizes the electrochemical data obtained from the cyclic voltammetry measurements of ligand **1** and complex **2**.

Computational Details. All calculations were performed at the density functional theory (DFT) level[25] using the M06-L local functional[26] as implemented in Gaussian 09.[27] Numerical integrations were performed with an ultrafine grid. An automatic density-fitting set generated by the Gaussian program was used to reduce computational cost. Geometry optimizations were performed in the gas phase using the def2-SVP basis sets.[28] The natures of all stationary points were confirmed by analytic computation of vibrational frequencies. Transition state structures were verified to connect with the corresponding reactants and products by following normal modes associated with their imaginary frequencies. All frequencies below 50 cm^{-1} were replaced by 50 cm^{-1} when computing vibrational partition functions.[29] Final free energies in solution were computed by adding gas-phase free energy contributions (298.15 K) to single-point calculations in THF solvent using the SMD model[30] and the def2-TZVPP basis sets.[28] For all species, a factor of $RT\cdot\ln(24.46)$ was included to take into account the 1 atm to 1 M standard-state free energy change. Additional single-point calculations were carried using the B3LYP-D3 hybrid functional (see Table S5).[31,32]

■ ASSOCIATED CONTENT

Supporting Information

The Supporting Information is available free of charge on the ACS Publications website at DOI: 10.1021/acs.organomet.6b00765.

Experimental procedures, spectral and crystallographic data, and computational details (PDF)
Cartesian coordinates for all optimized structures (XYZ)
Crystallographic data for **1**, **2**, and **2b** (CIF)

■ AUTHOR INFORMATION

Corresponding Authors

*E-mail, cramer@umn.edu. Twitter, @ChemProfCramer
*E-mail: kuzui@staff.uni-marburg.de.
*E-mail: ifernan@ual.es.

ORCID

Christopher J. Cramer: 0000-0001-5048-1859
Ignacio Fernández: 0000-0001-8355-580X

Present Address

P.O.-B.: Instituto de Tecnología Química, Universitat Politècnica de València-Consejo Superior de Investigaciones Científicas (UPV-CSIC), Avda. de los Naranjos s/n, 46022 Valencia, Spain.

Notes

The authors declare no competing financial interest.

■ ACKNOWLEDGMENTS

This work was supported by the Junta de Andalucía (Spain) under the project number P12-FQM-2668, the U.S. National Science Foundation (CHE-1361595) and by Bruker Española SA. A.R.-B. and P.O.-B. thank the University of Almería and MEC for a Ph.D. fellowship and a Ramón y Cajal contract (RYC-2014-16620), respectively. R.L. is funded by the DFG (LA 2830/3-2). I.K. would like to thank Prof. S. Dehnen for generous support and Prof. B. Neumüller for X-ray measurements of **2** and **2b**. We acknowledge the Minnesota Supercomputing Institute (MSI) at the University of Minnesota for providing resources that contributed to the research results reported within this paper.

■ REFERENCES

(1) (a) Marciniec, B.; Gulinski, J.; Urbaniak, W.; Kornetka, Z. W. *Comprehensive Handbook on Hydrosilylation*; Pergamon Press: Oxford, U.K., 1992;. (b) Roy, A. K. *Adv. Organomet. Chem.* **2007**, *55*, 1−59. (c) Marciniec, B., Ed. *Hydrosilylation: A Comprehensive Review on Recent Advances*; Springer: Dordrecht, The Netherlands, 2009.

(2) (a) Marciniec, B.; Gulinsky, J.; Urbaniak, W.; Kornetka, Z. W. In *Comprehensive Handbook on Hydrosilylation*; Marciniec, B., Ed.; Pergamon: Oxford, 1992. (b) Marciniec, B., Ed. *Hydrosilylation: A Comprehensive Review on Recent Advances*; Springer: New York, 2009. For reviews of iron-catalyzed hydrosilylation: (c) Morris, R. H. *Chem. Soc. Rev.* **2009**, *38*, 2282−2291. (d) Zhang, M.; Zhang, A. *Appl. Organomet. Chem.* **2010**, *24*, 751−757. (e) Junge, K.; Schroder, K.; Beller, M. *Chem. Commun.* **2011**, *47*, 4849−4859.

(3) Selected reviews: (a) Bolm, C.; Legros, J.; Le Paih, J.; Zani, L. *Chem. Rev.* **2004**, *104*, 6217−6254. (b) Plietker, B., Ed. *Iron Catalysis in Organic Chemistry*; Wiley-VCH: Weinheim, Germany, 2008. (c) Zhang, M.; Zhang, A. *Appl. Organomet. Chem.* **2010**, *24*, 751−757. (d) Chakraborty, S.; Guan, H. *Dalton Trans.* **2010**, *39*, 7427−7436. (e) Le Bailly, B. A. F.; Thomas, S. P. *RSC Adv.* **2011**, *1*, 1435−1445. (f) Bullock, R. M. *Catalysis without precious metals*; Wiley-VCH: Weinheim, 2010. (g) Bullock, R. M. *Science* **2013**, *342*, 1054−1055. (h) Bauer, I.; Knolker, H.-J. *Chem. Rev.* **2015**, *115*, 3170−3387.

DOI: 10.1021/acs.organomet.6b00765
Organometallics XXXX, XXX, XXX−XXX

(i) Hoyt, J. M.; Schmidt, V. A.; Tondreau, A. M.; Chirik, P. J. *Science* **2015**, *349*, 960−963. (j) Yu, R. P.; Hesk, D.; Rivera, N.; Pelczer, I.; Chirik, P. J. *Nature* **2016**, *529*, 195−199.

(4) Selected references on Fe-catalyzed hydrosilylations: (a) Tondreau, A. M.; Darmon, J. M.; Wile, B. M.; Floyd, S. K.; Lobkovsky, E.; Chirik, P. J. *Organometallics* **2009**, *28*, 3928−3940. (b) Inagaki, T.; Ito, A.; Ito, J.; Nishiyama, H. *Angew. Chem., Int. Ed.* **2010**, *49*, 9384−9387. (c) Kandepi, V. V. K. M.; Cardoso, J. M. S.; Peris, E.; Royo, B. *Organometallics* **2010**, *29*, 2777−2782. (d) Yang, J.; Tilley, D. T. *Angew. Chem., Int. Ed.* **2010**, *49*, 10186−10188. (e) Bhattacharya, P.; Krause, J. A.; Guan, H. *Organometallics* **2011**, *30*, 4720−4729. (f) Buitrago, E.; Tinnis, F.; Adolfsson, H. *Adv. Synth. Catal.* **2012**, *354*, 217−222. (g) Ruddy, A. J.; Kelly, C. M.; Crawford, S. M.; Wheaton, C. A.; Sydora, O. L.; Small, B. L.; Stradiotto, M.; Turculet, L. *Organometallics* **2013**, *32*, 5581−5588. (h) Blom, B.; Enthaler, S.; Inoue, S.; Irran, E.; Driess, M. *J. Am. Chem. Soc.* **2013**, *135*, 6703−6713. (i) Zuo, Z.; Sun, H.; Wang, L.; Li, X. *Dalton Trans.* **2014**, *43*, 11716−11722. (j) Zuo, Z.; Zhang, L.; Leng, X.; Huang, Z. *Chem. Commun.* **2015**, *51*, 5073−5076. (k) Wekesa, F. S.; Arias-Ugarte, R.; Kong, L.; Sumner, Z.; McGovern, G. P.; Findlater, M. *Organometallics* **2015**, *34*, 5051−5056.

(5) Bleith, T.; Wadepohl, H.; Gade, L. H. *J. Am. Chem. Soc.* **2015**, *137*, 2456−2459.

(6) Nishiyama, H.; Furuta, A. *Chem. Commun.* **2007**, 760−762.

(7) Wang, W.; Gu, P.; Wang, Y.; Wei, H. *Organometallics* **2014**, *33*, 847−857.

(8) (a) Gallego, D.; Inoue, S.; Blom, B.; Driess, M. *Organometallics* **2014**, *33*, 6885−6897. (b) Metsänen, T. T.; Gallego, D.; Szilvási, T.; Driess, M.; Oestreich, M. *Chem. Sci.* **2015**, *6*, 7143−7149.

(9) Bleith, T.; Gade, L. H. *J. Am. Chem. Soc.* **2016**, *138*, 4972−4983.

(10) (a) da Cunha, C. J.; Fielder, S. S.; Stynes, D. V.; Masui, H.; Auburn, P. R.; Lever, A. B. P. *Inorg. Chim. Acta* **1996**, *242*, 293−302. (b) Ochiai, K.; Mazaki, Y.; Nishikiori, S.; Kobayashi, K.; Hayashi, S. *J. Chem. Soc., Perkin Trans. 2* **1996**, 1139−1145. (c) Joshi, B. S.; Rho, T.; Rinaldi, P. L.; Liu, W.; Wagler, T. A.; Newton, M. G.; Lee, D.; Pelletier, S. W. *J. Chem. Crystallogr.* **1991**, *27*, 553−559.

(11) For related examples, see Ghosh, C.; Groy, T. L.; Bowman, A. C.; Trovitch, R. J. *Chem. Commun.* **2016**, *52*, 4553−4556.

(12) Vergote, T.; Nahra, F.; Merschaert, A.; Riant, O.; Peeters, D.; Leyssens, T. *Organometallics* **2014**, *33*, 1953−1963.

(13) Ghosh, C.; Mukhopadhyay, T. K.; Flores, M.; Groy, T. L.; Trovitch, R. J. *Inorg. Chem.* **2015**, *54*, 10398−10406.

(14) Small spin contamination (<S^2> of ca. 6.4 instead of 6.0) was observed for [Fe] complexes, likely due to possible contribution of the anthraquinonic ligand to higher spin states.

(15) [Ti]: (a) Bandini, M.; Bernardi, F.; Bottoni, A.; Cozzi, P. G.; Miscione, G. P.; Umani-Ronchi, A. *Eur. J. Org. Chem.* **2003**, *2003*, 2972−2984. [Cu]: (b) Issenhuth, J.-T.; Notter, F.-P.; Dagorne, S.; Dedieu, A.; Bellemin-Laponnaz, S. *Eur. J. Inorg. Chem.* **2010**, *2010*, 529−541. (c) Vergote, T.; Gathy, T.; Nahra, F.; Riant, O.; Peeters, D.; Leyssens, T. *Theor. Chem. Acc.* **2012**, *131*, 1253.

(16) We have computed the species **4** and **TS4−5** using the actual silane, that is, $(EtO)_2MeSiH$. The relative activation free energy is 27.3 kcal mol^{-1}, which is essentially the same as the value reported for $(MeO)_2MeSiH$, 26.3 kcal mol^{-1}.

(17) Kozuch, S. *WIREs Comput. Mol. Sci.* **2012**, *2*, 795−815. Our value is estimated by considering both the catalytic cycle (hydrosilylation) energies and the initial catalyst activation step at 298 K.

(18) (a) Gómez-Gallego, M.; Sierra, M. A. *Chem. Rev.* **2011**, *111*, 4857−4963. (b) Christensen, N. J.; Fristrup, P. *Synlett* **2015**, *26*, 508−513.

(19) We note that H/D KIE might not be conclusive for distinguishing the rate-limiting character of various elementary steps as all of them involve hydride transfers. Instead, ^{13}C-KIE studies for the carbonyl carbon of acetophenone are in progress. We predict a value of 1.025 for ketone reduction through **TS6−7**.

(20) Andersen, R. A.; Faegri, K., Jr.; Green, J. C.; Haaland, A.; Lappert, M. F.; Leung, W.-P.; Rypdal, K. *Inorg. Chem.* **1988**, *27*, 1782−1786.

(21) (a) *APEX2*, version 2008.1−0; Bruker AXS Inc.: Madison, WI, 2008. (b) *SAINT. Data Reduction Software*, V6.28A; Bruker AXS Inc.: Madison, WI, 2001.

(22) Sheldrick, G. M. *SADABS. Program for Empirical Absorption Correction*; University of Gottingen: Gottingen, Germany, 1996.

(23) Altomare, A.; Burla, M. C.; Camalli, M.; Cascarano, G. L.; Giacovazzo, C.; Guagliardi, A.; Moliterni, A. G. G.; Polidori, G.; Spagna, R. *J. Appl. Crystallogr.* **1999**, *32*, 115−119.

(24) (a) Sheldrick, G. M. *Program for Crystal Structure Refinement*; University of Göttingen: Göttingen, Germany, 2014. (b) Farrugia, L. J. *J. Appl. Crystallogr.* **1999**, *32*, 837−838.

(25) Cramer, C. J.; Truhlar, D. G. *Phys. Chem. Chem. Phys.* **2009**, *11*, 10757−10816.

(26) (a) Zhao, Y.; Truhlar, D. G. *J. Chem. Phys.* **2006**, *125*, 194101. (b) Zhao, Y.; Truhlar, D. G. *Acc. Chem. Res.* **2008**, *41*, 157−167. (c) Zhao, Y.; Truhlar, D. G. *Chem. Phys. Lett.* **2011**, *502*, 1−13.

(27) Frisch, M. J.; Trucks, G. W.; Schlegel, H. B.; Scuseria, G. E.; Robb, M. A.; Cheeseman, J. R.; Scalmani, G.; Barone, V.; Mennucci, B.; Petersson, G. A.; Nakatsuji, H.; Caricato, M.; Li, X.; Hratchian, H. P.; Izmaylov, A. F.; Bloino, J.; Zheng, G.; Sonnenberg, J. L.; Hada, M.; Ehara, M.; Toyota, K.; Fukuda, R.; Hasegawa, J.; Ishida, M.; Nakajima, T.; Honda, Y.; Kitao, O.; Nakai, H.; Vreven, T.; Montgomery, J. A., Jr.; Peralta, J. E.; Ogliaro, F.; Bearpark, M.; Heyd, J. J.; Brothers, E.; Kudin, K. N.; Staroverov, V. N.; Kobayashi, R.; Normand, J.; Raghavachari, K.; Rendell, A.; Burant, J. C.; Iyengar, S. S.; Tomasi, J.; Cossi, M.; Rega, N.; Millam, J. M.; Klene, M.; Knox, J. E.; Cross, J. B.; Bakken, V.; Adamo, C.; Jaramillo, J.; Gomperts, R.; Stratmann, R. E.; Yazyev, O.; Austin, A. J.; Cammi, R.; Pomelli, C.; Ochterski, J. W.; Martin, R. L.; Morokuma, K.; Zakrzewski, V. G.; Voth, G. A.; Salvador, P.; Dannenberg, J. J.; Dapprich, S.; Daniels, A. D.; Farkas, O.; Foresman, J. B.; Ortiz, J. V.; Cioslowski, J.; Fox, D. J. *Gaussian 09*, revision D.01; Gaussian, Inc.: Wallingford, CT, 2009.

(28) Weigend, F.; Ahlrichs, R. *Phys. Chem. Chem. Phys.* **2005**, *7*, 3297−3305.

(29) Ribeiro, R. F.; Marenich, A. V.; Cramer, C. J.; Truhlar, D. G. *J. Phys. Chem. B* **2011**, *115*, 14556.

(30) Marenich, A. V.; Cramer, C. J.; Truhlar, D. G. *J. Phys. Chem. B* **2009**, *113*, 6378−6396.

(31) (a) Becke, A. D. *Phys. Rev. A: At., Mol., Opt. Phys.* **1988**, *38*, 3098−3100. (b) Lee, C.; Yang, W.; Parr, R. G. *Phys. Rev. B: Condens. Matter Mater. Phys.* **1988**, *37*, 785−789. (c) Stephens, P. J.; Devlin, F. J.; Chabalowski, C. F.; Frisch, M. J. *J. Phys. Chem.* **1994**, *98*, 11623.

(32) Grimme, S.; Antony, J.; Ehrlich, S.; Krieg, H. *J. Chem. Phys.* **2010**, *132*, 154104.

DOI: 10.1021/acs.organomet.6b00765
Organometallics XXXX, XXX, XXX−XXX